Transp Porous Med (2012) 91:813–831
DOI 10.1007/s11242-011-9874-y

Matched Boundary Extrapolation Solutions for CO_2 Well-Injection into a Saline Aquifer

J. E. Houseworth

Received: 26 April 2011 / Accepted: 8 September 2011 / Published online: 30 September 2011

Abstract The injection of supercritical CO_2 through wells into deep brine reservoirs is a topic of interest for geologic carbon sequestration. The injected CO_2 is predominantly immiscible with the brine and its low density relative to brine leads to strong buoyancy effects. The displacement of brine by CO_2 in general is a multidimensional, complex nonlinear problem that requires numerical methods to solve. The approximations of vertical equilibrium and complete gravity segregation (sharp interface) have been introduced to reduce the complexity and dimensionality of the problem. Furthermore, for the radial displacement process considered here, the problem can be formulated in terms of a similarity variable that reduces spatial and temporal dependencies to a single variable. However, the resulting ordinary differential equation is still nonlinear and exact solutions are not available. The existing analytical solutions are approximations limited to certain parameter ranges that become inaccurate over a large portion of the parameter space. Here, I use a matched boundary extrapolation method to provide much greater accuracy for analytical/semi-analytical approximations over the full parameter range.

Keywords CO_2 sequestration · Vertical equilibrium · Gravity segregation · Analytical solution

1 Introduction

The connection identified between atmospheric emissions of CO_2 and global climate change has led to intensive investigations of ways to reduce the build-up of CO_2 in the atmosphere. One mitigation strategy is called geologic carbon sequestration, where CO_2 is injected into permeable geologic formations to prevent CO_2 emissions from entering the atmosphere. The two main types of target formations are depleted (or depleting) oil reservoirs and deep saline

J. E. Houseworth (✉)
Division of Earth Sciences, Lawrence Berkeley National Laboratory,
1 Cyclotron Road, Berkeley, CA 94720, USA
e-mail: jehouseworth@lbl.gov

aquifers. This article focuses on processes associated with CO_2 injection into deep saline aquifers.

Typically, CO_2 is injected into receiving formations through wells sufficiently deep (generally 800 m is sufficient) such that the CO_2 is in a supercritical state. Brine and CO_2 may be approximated as immiscible phases although there is a small degree of solubility of CO_2 in brine and water in CO_2 (IPCC 2005). Given sufficient time, on the order of hundreds of years (IPCC 2005), the mutual solubility can have a significant effect; however, for shorter times the solubility effect is small. For supercritical conditions, CO_2 is much denser than air but still less dense than formation brine and has a lower viscosity than brine. The buoyancy of the CO_2 relative to brine leads to a tendency for the CO_2 to override the brine along the caprock sealing the aquifer.

The immiscible displacement problem for flow from a well has been investigated using both analytical and numerical methods (Nordbotten et al. 2005; Nordbotten and Celia 2006; Dentz and Tartakovsky 2009a; Liu et al. 2010). Nordbotten et al. (2005) used an energy minimization approach to determine the displacement profile for cases having negligible buoyancy effects and significant buoyancy effects. The results are given in terms of an analytical relationship for the case in which buoyancy is negligible and a semi-analytical relationship for when buoyancy is important. However, the validity of the energy minimization approach was later questioned by Nordbotten and Celia (2006) and Dentz and Tartakovsky (2009a). Nordbotten and Celia (2006) analyzed the CO_2 injection problem using vertical equilibrium, sharp interface approximations, and recast the problem in terms of a similarity variable. The similarity transformation reduces the partial differential equation governing the displacement profile to an ordinary differential equation. An analytical solution was found for the case with negligible buoyancy. The case in which buoyancy is important required numerical solutions of the nonlinear ordinary differential equation.

Dentz and Tartakovsky (2009a) developed an approximate analytical solution for CO_2 injection through a well. This solution was obtained using the hypothesis that the volumetric flow rates for CO_2 and brine are proportional to the depth of the aquifer occupied by each phase at a given radius from the well. However, the validity of this hypothesis, including the effects of parameter variations on the suitability of the approximate solution, was not investigated.

Liu et al. (2010) investigated the CO_2 well-injection problem using the sharp interface approximation but without the vertical equilibrium approximation. Numerical solution of the governing equations was required. Results were compared with solutions using the similarity model of Nordbotten and Celia (2006). In general, the two methods were in reasonable agreement, with the largest discrepancies occurring along the top of the aquifer where CO_2 penetration is the greatest.

Here, I present and analyze the problem of injection/release of CO_2 from a well into a confined saline aquifer. The problem is limited to cases in which the aquifer may be approximated as horizontal and where other flow effects, such as regional groundwater flow, are small such that the displacement pattern is radially symmetric around the well. The governing equation is developed using the vertical equilibrium approximation which assumes a static pressure distribution; therefore, the resulting flow field is approximated as entirely horizontal. An assumption of complete gravity segregation is also used, which posits that only one phase is flowing at any location. This assumption allows for the development of the governing equation in terms of the free interface height. The theoretical basis for both of these approximations is discussed in detail by Yortsos (1995) for a linear flow system. Further analysis is provided here regarding the application of these approximations to a radial flow system. Compressibility effects are not included in this analysis; however, Vilarrasa et al.

(2010) discuss compressibility effects for the CO_2 well-injection problem and provide an approximate method by which to correct for compressibility effects in models that assume incompressibility. The governing equation may be expressed in terms of a similarity variable, as described by Nordbotten and Celia (2006), for the case of a constant rate injection into an initially undisturbed aquifer. This reduces the partial differential equation expressed in terms of radial distance and time to an ordinary differential equation expressed in terms of a Boltzmann-type similarity variable.

The transformed equation is a nonlinear two-point boundary value problem. New approximate analytical and semi-analytical solutions are obtained through a matched boundary extrapolation (MBE) method. The MBE method involves developing approximate solutions expected to be accurate at the system boundaries. These boundary solutions are then extrapolated to an interior point where they are matched and constrained to ensure mass balance. The MBE solutions are investigated over a wide range of dimensionless parameters associated with the problem and compared with solutions of other investigators.

2 The Vertical Equilibrium and Gravity Segregation Approximations

A dimensional analysis for displacement of brine by CO_2 in a radial flow system is developed here to evaluate the conditions under which vertical equilibrium and gravity segregation may be expected to be reasonable approximations. This is similar to the analysis presented by Yortsos (1995) for a linear flow system, but addresses the differences inherent to a radial flow system.

Fluids and rock are treated as incompressible relative to the displacement of brine by CO_2, such that the divergence of the total flow field is approximately zero. The reservoir boundaries are horizontal, and there is no regional flow; flow is entirely a result of CO_2 entering the formation from the well. The system is assumed to be homogeneous and horizontally isotropic; anisotropy in permeability is included for the vertical direction.

The evaluation requires scaling the equations for incompressibility and Darcy's law for each phase, as given in Eqs. 1 through 3:

$$\frac{1}{r}\frac{\partial}{\partial r}\left\{r\left(u_{\mathrm{n}r}\left(r,z,t\right)+u_{\mathrm{w}r}\left(r,z,t\right)\right)\right\}+\frac{\partial}{\partial z}\left(u_{\mathrm{n}z}\left(r,z,t\right)+u_{\mathrm{w}z}\left(r,z,t\right)\right)=0, \tag{1}$$

$$\boldsymbol{u}_{\mathrm{n}}\left(r,z,t\right)=-\frac{k_{r\mathrm{w}}\left(S_{\mathrm{w}}\left(r,z,t\right)\right)}{\mu_{\mathrm{n}}}\left\{k_h\frac{\partial p_{\mathrm{n}}}{\partial r}\left(r,z,t\right)\boldsymbol{\mathcal{R}}+k_z\left(\frac{\partial p_{\mathrm{n}}}{\partial z}\left(r,z,t\right)+\rho_{\mathrm{n}}g\right)\boldsymbol{\kappa}\right\}, \tag{2}$$

$$\boldsymbol{u}_{\mathrm{w}}\left(r,z,t\right)=-\frac{k_{r\mathrm{w}}\left(S_{\mathrm{w}}\left(r,z,t\right)\right)}{\mu_{\mathrm{w}}}\left\{k_h\frac{\partial p_{\mathrm{w}}}{\partial r}\left(r,z,t\right)\boldsymbol{\mathcal{R}}+k_z\left(\frac{\partial p_{\mathrm{w}}}{\partial z}\left(r,z,t\right)+\rho_{\mathrm{w}}g\right)\boldsymbol{\kappa}\right\}. \tag{3}$$

The fluid fluxes of CO_2 and brine are $\boldsymbol{u}_{\mathrm{n}}$ and $\boldsymbol{u}_{\mathrm{w}}$, respectively, where bolding indicates a vector quantity. The subscript "n" refers to CO_2 as a non-wetting phase and "w" refers to brine as the wetting phase. The saturation of brine is denoted by s_{w}, which is the volumetric fraction of pore space occupied by brine. The CO_2 and brine fluid pressures are p_{n} and p_{w}, respectively. The horizontal and vertical permeabilities are k_h and k_z, respectively. The relative permeabilities for CO_2 and brine are given by $k_{r\mathrm{n}}\left(S_{\mathrm{w}}\right)$ and $k_{r\mathrm{w}}\left(s_{\mathrm{w}}\right)$, which are homogeneous and isotropic. The CO_2 and brine phase viscosities are μ_{n} and μ_{w}, respectively, and their respective densities are ρ_{n} and ρ_{w}. The gravitational acceleration is g, the

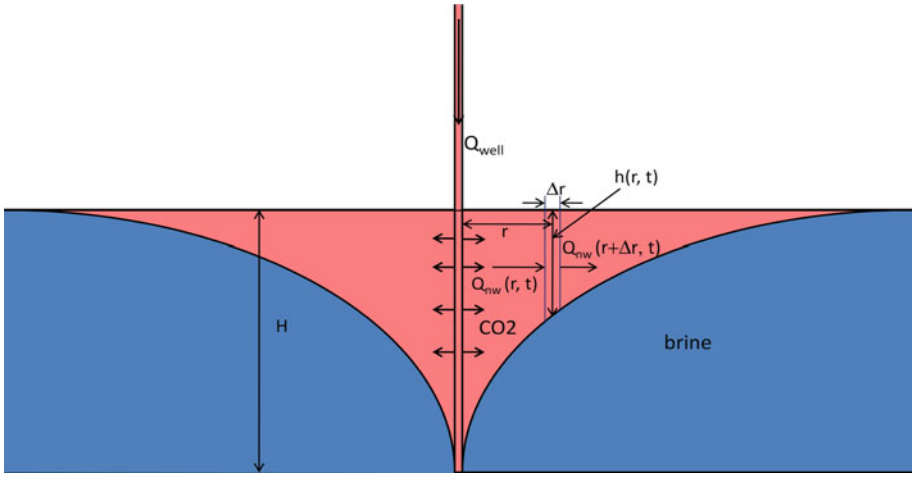

Fig. 1 Definition diagram for CO_2 flow from a well into a saline aquifer

radial unit vector is $\boldsymbol{\mathcal{R}}$, and the unit vector in the vertical direction is $\boldsymbol{\kappa}$. The radial and vertical coordinates are r and z, respectively, as shown in Fig. 1.

An auxillary relationship for capillary pressure is:

$$p_{\mathrm{c}}\left(S_{\mathrm{w}}\right) = p_{\mathrm{n}} - p_{\mathrm{w}}, \tag{4}$$

where p_{c} is the capillary pressure.

Equations 1 through 4 may be used in a dimensional analysis to help understand what is meant by the vertical equilibrium and gravity segregation approximations. The analysis proceeds by developing dimensional groups representative of the various quantities in Eqs. 1 through 4, so that these equations may be put into a dimensionless form. Length scales for the vertical and radial directions are denoted by H and $L\,(t)$, respectively. The aquifer thickness is given by H; however, unlike the problem analyzed by Yortsos (1995), there is no unique length scale for the radial direction. Both the saturation and pressure fields expand radially in proportion to the square root of time (Nordbotten and Celia 2006). Therefore, $L\,(t)$ is taken to be proportional to the square root of time, consistent with the evolution of the system.

There is no unique scaling for the flux terms $\boldsymbol{u}_{\mathrm{n}}$ and $\boldsymbol{u}_{\mathrm{w}}$ because of the overall decrease in flux with radial distance from the well. However, the flow rate per unit depth for CO_2 and brine, $\boldsymbol{q}_{\mathrm{n}}$ and $\boldsymbol{q}_{\mathrm{w}}$, defined as

$$\boldsymbol{q}_{\mathrm{n}}\left(r, z, t\right) = 2\pi r \boldsymbol{u}_{\mathrm{n}}\left(r, z, t\right), \tag{5}$$

$$\boldsymbol{q}_{\mathrm{w}}\left(r, z, t\right) = 2\pi r \boldsymbol{u}_{\mathrm{w}}\left(r, z, t\right), \tag{6}$$

can be scaled. The scaling variable for flow rate per unit depth, q_{s}, is given by

$$q_{\mathrm{s}} = \frac{Q_{\mathrm{well}}}{H}. \tag{7}$$

To scale the pressure, consider the single-phase relationship for CO_2 flow from a well at a rate Q_{well}

$$Q_{\mathrm{well}} = -2\pi r H \frac{k_h}{\mu_{\mathrm{n}}} \frac{\partial p}{\partial r}, \tag{8}$$

which leads to the following definition of the pressure scale, p_s:

$$p_{\mathrm{s}} = \frac{\mu_{\mathrm{n}} Q_{\mathrm{well}}}{2\pi k_h H}. \tag{9}$$

Finally, define the capillary pressure scale, p_{cs}, as

$$p_{\mathrm{cs}} = \frac{\sigma \cos(\theta)}{\sqrt{\frac{k_h}{\phi}}}, \tag{10}$$

which is the Leverrett J-function normalization (Bear 1972) for capillary pressure, where σ is the CO_2-brine surface tension, θ is the contact angle between the CO_2-brine interface and the rock surface as measured through the brine, and ϕ is the rock porosity.

2.1 Evaluation of Vertical Equilibrium

Using the definitions (5) and (6) in (1) gives

$$\frac{Q_{\mathrm{well}}}{2\pi L^2 H \hat{r}} \frac{\partial\left(\hat{q}_{\mathrm{n}r} + \hat{q}_{\mathrm{w}r}\right)}{\partial \hat{r}} + \frac{Q_{\mathrm{well}}}{2\pi L H^2 \hat{r}} \frac{\partial\left(\hat{q}_{\mathrm{n}z} + \hat{q}_{\mathrm{w}z}\right)}{\partial \hat{z}} = 0, \tag{11}$$

where the flow rates per unit depth are scaled using (7), which gives the dimensionless variables $\hat{\boldsymbol{q}}_{\mathrm{n}} = \frac{2\pi r H}{Q_{\mathrm{well}}} \boldsymbol{u}_{\mathrm{n}}$ and $\hat{\boldsymbol{q}}_{\mathrm{w}} = \frac{2\pi r H}{Q_{\mathrm{well}}} \boldsymbol{u}_{\mathrm{w}}$. The radial and vertical coordinates are scaled by L and H, respectively, which gives the dimensionless variables $\hat{r} = \frac{r}{L}$; $\hat{z} = \frac{z}{H}$.

Let the total flow rate per unit depth be $\hat{\boldsymbol{q}} = \hat{\boldsymbol{q}}_{\mathrm{n}} + \hat{\boldsymbol{q}}_{\mathrm{w}}$. Equation 11 then becomes,

$$\epsilon \frac{\partial \hat{q}_r}{\partial \hat{r}} + \frac{\partial \hat{q}_z}{\partial \hat{z}} = 0, \tag{12}$$

where $\epsilon = \frac{H}{L}$. Using the scaling variables the radial component of (2) becomes

$$\hat{q}_{\mathrm{n}r} = -k_{r\mathrm{w}} \hat{r} \frac{\partial \hat{p}_{\mathrm{n}}}{\partial \hat{r}}, \tag{13}$$

where the dimensionless CO_2 pressure is $\hat{p}_{\mathrm{n}} = \frac{2\pi k_h H}{\mu_{\mathrm{n}} Q_{\mathrm{well}}} p_{\mathrm{n}}$. Scaling the vertical component of (2) gives

$$\frac{\epsilon}{\delta} \hat{q}_{\mathrm{n}z} = -k_{r\mathrm{n}} \hat{r} \left(\frac{\partial \hat{p}_{\mathrm{n}}}{\partial \hat{z}} + \epsilon \frac{2\pi \rho_{\mathrm{n}} g H L k_h}{\mu_{\mathrm{n}} Q_{\mathrm{well}}} \right), \tag{14}$$

where $\delta = \frac{k_v}{k_h}$. Similarly, for the horizontal and vertical components of brine flow in (3),

$$\hat{q}_{\mathrm{w}r} = -k_{r\mathrm{w}} \frac{\mu_{\mathrm{n}}}{\mu_{\mathrm{w}}} \hat{r} \frac{\partial \hat{p}_{\mathrm{w}}}{\partial \hat{r}}, \tag{15}$$

$$\frac{\epsilon}{\delta} \hat{q}_{\mathrm{w}z} = -k_{r\mathrm{w}} \hat{r} \left(\frac{\mu_{\mathrm{n}}}{\mu_{\mathrm{w}}} \frac{\partial \hat{p}_{\mathrm{w}}}{\partial \hat{z}} + \epsilon \frac{2\pi \rho_{\mathrm{w}} g H L k_h}{\mu_{\mathrm{w}} Q_{\mathrm{well}}} \right). \tag{16}$$

Taking the sum of the flow rates per unit depth for CO_2 and brine gives the total flow rates per unit depth in the radial and vertical directions

$$\hat{q}_r = -k_{r\mathrm{n}}(S_{\mathrm{w}}) \hat{r} \frac{\partial \hat{p}_{\mathrm{n}}}{\partial \hat{r}} - k_{r\mathrm{w}}(S_{\mathrm{w}}) \frac{\mu_{\mathrm{n}}}{\mu_{\mathrm{w}}} \hat{r} \frac{\partial \hat{p}_{\mathrm{w}}}{\partial \hat{r}}, \tag{17}$$

$$\frac{\epsilon}{\delta} \hat{q}_z = -k_{r\mathrm{n}} \hat{r} \left(\frac{\partial \hat{p}_{\mathrm{n}}}{\partial \hat{z}} + \epsilon \frac{2\pi \rho_{\mathrm{n}} g H L k_h}{\mu_{\mathrm{n}} Q_{\mathrm{well}}} \right) - k_{r\mathrm{w}} \hat{r} \left(\frac{\mu_{\mathrm{n}}}{\mu_{\mathrm{w}}} \frac{\partial \hat{p}_{\mathrm{w}}}{\partial \hat{z}} + \epsilon \frac{2\pi \rho_{\mathrm{w}} g H L k_h}{\mu_{\mathrm{w}} Q_{\mathrm{well}}} \right). \tag{18}$$

As the parameter $\epsilon \to 0$, (12) indicates that that magnitude of $\hat{q}_z$ must be proportional to ϵ. Otherwise, the incompressibility condition cannot be met. Therefore, $\hat{q}_z = \epsilon \hat{\mathrm{w}}_z$, where $\hat{\mathrm{w}}_z$ is of the same order as $\hat{q}_r$ Substituting this into (18) gives

$$\frac{\epsilon^2}{\delta}\widehat{\mathrm{w}}_z = -k_{rn}\hat{r}\left(\frac{\partial \hat{p}_\mathrm{n}}{\partial \hat{z}} + \epsilon\frac{2\pi\rho_\mathrm{n} g H L k_h}{\mu_\mathrm{n} Q_\mathrm{well}}\right) - k_{rw}\hat{r}\left(\frac{\mu_\mathrm{n}}{\mu_\mathrm{w}}\frac{\partial \hat{p}_\mathrm{w}}{\partial \hat{z}} + \epsilon\frac{2\pi\rho_\mathrm{w} g H L k_h}{\mu_\mathrm{w} Q_\mathrm{well}}\right). \quad (19)$$

When $\frac{\epsilon^2}{\delta} \to 0$, (19) requires that the terms in parentheses multiplying the relative permeability terms must go to zero because the relative permeabilities are independent parameter functions. Each of these terms is zero when the vertical pressure gradient equals the static gradient. A static vertical pressure gradient within each phase is the definition of vertical equilibrium. Yortsos (1995) found the same parameter requirement, $\frac{\epsilon^2}{\delta} \to 0$, for vertical equilibrium in linear flow. Because the radial length scale, $L\,(t)$, increases with time, $\epsilon \to 0$ as $t \to \infty$. Therefore, the CO_2—brine displacement process will always tend to a vertical equilibrium condition after a sufficiently long time. Nordbotten and Celia (2006) reached a similar conclusion concerning the applicability of vertical equilibrium as a function of time.

2.2 Evaluation of Gravity Segregation and Capillary Effects

The approximations that capillary forces are negligible and that the fluids are gravity-segregated can be evaluated from (17) and (19). Starting with (19) for vertical flow, rearrange terms to isolate the capillary pressure and buoyancy effects:

$$\begin{aligned}\frac{\epsilon^2}{\delta}\widehat{\mathrm{w}}_z = &-\left(k_{rn} + k_{rw}\frac{\mu_\mathrm{n}}{\mu_\mathrm{w}}\right)\hat{r}\left(\frac{\partial \hat{p}_\mathrm{n}}{\partial \hat{z}} + \epsilon\frac{2\pi\rho_\mathrm{n} g H L k_h}{\mu_\mathrm{n} Q_\mathrm{well}}\right)\\ &+k_{rw}\hat{r}\left(\frac{\mu_\mathrm{n}}{\mu_\mathrm{w}}\frac{\partial\left(\hat{p}_\mathrm{n} - \hat{p}_\mathrm{w}\right)}{\partial \hat{z}} - \epsilon\frac{2\pi\left(\rho_\mathrm{w} - \rho_\mathrm{n}\right) g H L k_h}{\mu_\mathrm{w} Q_\mathrm{well}}\right). \quad (20)\end{aligned}$$

Using (14) to eliminate the second term in parentheses on the right-hand side of (20) gives:

$$\begin{aligned}\frac{\epsilon^2}{\delta}\widehat{\mathrm{w}}_z = &\left(k_{rn} + \frac{k_{rw}}{k_{rn}}\frac{\mu_\mathrm{n}}{\mu_\mathrm{w}}\right)\frac{\epsilon}{\delta}\hat{q}_{\mathrm{n}z}\\ &+k_{rw}\hat{r}\left(\frac{\mu_\mathrm{n}}{\mu_\mathrm{w}}\frac{\partial\left(\hat{p}_n - \hat{p}_w\right)}{\partial \hat{z}} - \epsilon\frac{2\pi\left(\rho_\mathrm{w} - \rho_\mathrm{n}\right) g H L k_h}{\mu_\mathrm{w} Q_\mathrm{well}}\right). \quad (21)\end{aligned}$$

Using (4), (9), and (10) in (21) gives:

$$\begin{aligned}\frac{\epsilon^2}{\delta}\widehat{\mathrm{w}}_z = &\left(k_{rn} + \frac{k_{rw}}{k_{rn}}\frac{\mu_\mathrm{n}}{\mu_\mathrm{w}}\right)\frac{\epsilon}{\delta}\hat{q}_{\mathrm{n}z}\\ &+k_{rw}\hat{r}\left(\frac{2\pi k_h H}{\mu_\mathrm{w} Q_\mathrm{well}}\frac{\sigma\cos(\theta)}{\sqrt{\frac{k_h}{\phi}}}\frac{\partial \hat{p}_\mathrm{c}}{\partial \hat{z}} - \epsilon\frac{2\pi\left(\rho_\mathrm{w} - \rho_\mathrm{n}\right) g H L k_h}{\mu_\mathrm{w} Q_\mathrm{well}}\right). \quad (22)\end{aligned}$$

Rearranging terms in (22) and solving for $\hat{q}_{\mathrm{n}z}$:

$$\begin{aligned}\hat{q}_{\mathrm{n}z} = &\epsilon\widehat{\mathrm{w}}_z\left(\frac{k_{rn}/\mu_\mathrm{n}}{k_{rn}/\mu_\mathrm{n} + k_{rw}/\mu_\mathrm{w}}\right)\\ &-2\pi\delta\frac{\left(\rho_\mathrm{w} - \rho_\mathrm{n}\right) g H L k_h k_{rw}}{\mu_\mathrm{w} Q_\mathrm{well}}\hat{r}\left(\frac{\frac{k_{rn}}{\mu_\mathrm{n}}}{\frac{k_{rn}}{\mu_\mathrm{n}} + \frac{k_{rw}}{\mu_\mathrm{w}}}\right)\left(\frac{1}{B}\frac{\partial \hat{p}_\mathrm{c}}{\partial \hat{z}} - 1\right), \quad (23)\end{aligned}$$

where

$$B = \frac{(\rho_w - \rho_n)\, g H}{\sigma \cos(\theta)} \sqrt{\frac{k_h}{\phi}} \tag{24}$$

is the Bond number (Nordbotten and Dahle 2010). The Bond number is a standard scaling relationship for evaluating the relative significance of capillary and gravitational forces. From (23) capillary pressure effects are negligible if the term multiplying the capillary pressure gradient is small compared with the buoyancy term, i.e., if $B \gg 1$. However, unlike vertical equilibrium, the relative strength of capillarity to gravity affecting the vertical movement of fluid does not diminish with increasing time.

If capillarity is negligible relative to gravity effects then (23) becomes

$$\hat{q}_{nz} = \epsilon \left[\widehat{w}_z \left(\frac{k_{rn}/\mu_n}{k_{rn}/\mu_n + k_{rw}/\mu_w} \right) + \hat{r} \left(\frac{k_{rw} k_{rn}/\mu_n}{k_{rn}/\mu_n + k_{rw}/\mu_w} \right) \frac{\delta}{\epsilon^2} \left(\frac{2\pi\, (\rho_w - \rho_n)\, g H^2 k_h}{\mu_w Q_{well}} \right) \right]. \tag{25}$$

Now $\frac{\epsilon^2}{\delta} \to 0$ is the condition that leads to vertical equilibrium. The dimensionless grouping $\frac{2\pi(\rho_w - \rho_n) g H^2 k_h}{\mu_w Q_{well}}$ represents the relative strength of buoyancy and viscous forces. If $\frac{2\pi(\rho_w - \rho_n) g H^2 k_h}{\mu_w Q_{well}} \sim O(1)$, buoyancy is not negligible and the last term on the right hand side of (25) diverges as $\frac{\delta}{\epsilon^2} \to \infty$. This term cannot be balanced by other terms in the equation, which are of smaller order. The only way to balance Eq. 25 when $\frac{2\pi(\rho_w - \rho_n) g H^2 k_h}{\mu_w Q_{well}} \sim O(1)$ is for $k_{rw}(S_w)\, k_{rn}(S_w) = 0$.

This is the condition of flow segregation, i.e., only one phase is flowing at a given location and time. Yortsos (1995) found a similar requirement for gravity segregation in linear flow. However, for radial flow, the condition favoring gravity segregation becomes stronger with time because $L \to \infty$ (and $\in \to 0$) and as $t \to \infty$.

If capillarity is not negligible with respect to buoyancy, then (23) indicates that gravity segregation will be weakened, because the opposing effects of buoyancy and capillarity help to balance the equation.

For radial motion, start with (17), rearrange terms to isolate capillary pressure effects and use (14) to eliminate the CO_2 pressure gradient/gravity term, to give

$$\hat{q}_r = \left(1 + \frac{k_{rw}}{k_{rn}} \frac{\mu_n}{\mu_w}\right) \hat{q}_{nr} + k_{rw} \frac{\mu_n}{\mu_w} \hat{r} \frac{\partial \left(\hat{p}_n - \hat{p}_w\right)}{\partial \hat{r}}, \tag{26}$$

and using (4), (9), and (10) in (26) and solving for $\hat{q}_{nr}$ gives

$$\hat{q}_{nr} = \left(\frac{k_{rn}/\mu_n}{k_{rn}/\mu_n + k_{rw}/\mu_w} \right) \hat{q}_r + \left(\frac{k_{rw} k_{rn}/\mu_n}{k_{rn}/\mu_n + k_{rw}/\mu_w} \right) \frac{2\pi\sigma\cos(\theta)\sqrt{\phi k_h} H}{\mu_w Q_{well}} \hat{r} \frac{\partial \hat{p}_c}{\partial \hat{r}}. \tag{27}$$

The term containing the capillary pressure is multiplied by $k_{rw}(S_w)\, k_{rn}(S_w)$, which is zero for a condition of gravity segregation. Therefore capillary effects in the radial direction are negligible under a condition of gravity segregation.

3 Governing Equation for Radial Displacement of Brine by CO_2

Now that the conditions for vertical equilibrium and gravity segregation have been established, the equation for the displacement of brine by CO_2 injected from a well can be derived by writing material balance equations using these approximations. The development of the governing equation follows that of Nordbotten and Celia (2006), but for completeness is included here. As shown in Fig. 1, if considering material balance over a small element,

$$2\pi r\phi\left(1-S_{\mathrm{wr}}\right)\frac{\partial h}{\partial t}\left(r,t\right)=-\frac{\partial Q_{\mathrm{n}}}{\partial r}\left(r,t\right), \tag{28}$$

$$2\pi r\phi\left(1-S_{\mathrm{wr}}\right)\frac{\partial h}{\partial t}\left(r,t\right)=\frac{\partial Q_{\mathrm{w}}}{\partial r}\left(r,t\right), \tag{29}$$

where h is the depth of flow of CO_2, ϕ is the porosity, S_{wr} is the residual saturation of brine following displacement by CO_2 and Q_{n} and Q_{w} are the radial flow rates of CO_2 and brine, respectively.

Darcy's law for horizontal, radial flow in each phase is:

$$Q_{\mathrm{n}}\left(r,t\right)=-2\pi rh\frac{k_{\mathrm{nr}}}{\mu_{\mathrm{n}}}\frac{\partial p_{\mathrm{n}}}{\partial r}\left(r,t\right), \tag{30}$$

$$Q_{\mathrm{w}}\left(r,t\right)=-2\pi r\left(H-h\right)\frac{k_{\mathrm{w}}}{\mu_{\mathrm{w}}}\frac{\partial p_{\mathrm{w}}}{\partial r}\left(r,t\right), \tag{31}$$

where p_{n} is the CO_2 pressure at the top of the reservoir, p_{w} is the brine pressure at the base of the reservoir, k_{nr} is the horizontal permeability to CO_2 at residual brine saturation, and k_{w} is the horizontal saturated permeability of brine. As a result of complete gravity segregation, all mobile brine has been displaced by CO_2 in the region with mobile CO_2. However, a residual, immobile brine saturation that cannot be displaced by CO_2 remains such that the CO_2 permeability in this region is the permeability to CO_2 at residual brine saturation. The region with mobile brine is ahead of the CO_2 displacement front and is completely saturated with brine; therefore, the brine permeability in this region is equal to the saturated brine permeability.

Using vertical static equilibrium, the CO_2 pressure at the top of the reservoir, p_{nw}, can be expressed in terms of the pressure of the brine at the base of the reservoir, p_{w}:

$$p_{\mathrm{n}}=p_{\mathrm{w}}-\rho_{\mathrm{w}}g\left(H-h\right)-\rho_{\mathrm{n}}gh=p_{\mathrm{w}}+\Delta\rho gh-\rho_{\mathrm{w}}gH. \tag{32}$$

The sum of the flow rates in (30) and (31) gives the well flow rate, Q_{well}:

$$Q_{\mathrm{well}}=-2\pi rh\frac{k_{\mathrm{nr}}}{\mu_{\mathrm{n}}}\frac{\partial p_{\mathrm{n}}}{\partial r}-2\pi r\left(H-h\right)\frac{k_{\mathrm{w}}}{\mu_{\mathrm{w}}}\frac{\partial p_{\mathrm{w}}}{\partial r}. \tag{33}$$

Using (32) for p_{n} in (33) gives

$$Q_{\mathrm{well}}=-2\pi rh\frac{k_{\mathrm{nr}}}{\mu_{\mathrm{n}}}\left(\frac{\partial p_{\mathrm{w}}}{\partial r}+\Delta\rho g\frac{\partial h}{\partial r}\right)-2\pi r\left(H-h\right)\frac{k_{\mathrm{w}}}{\mu_{\mathrm{w}}}\frac{\partial p_{\mathrm{w}}}{\partial r}. \tag{34}$$

Rearranging (34) to solve for the pressure gradient, substituting into (31) and then using the resulting expression for Q_{w} in (29), gives

$$\frac{\partial h}{\partial t}=\frac{1}{2\pi r\phi\left(1-S_{\mathrm{wr}}\right)}\frac{\partial}{\partial r}\left\{\frac{2\pi rh\left(H-h\right)\frac{k_{\mathrm{w}}}{\mu_{\mathrm{w}}}\frac{k_{\mathrm{nr}}}{\mu_{\mathrm{n}}}\Delta\rho g\frac{\partial h}{\partial r}+\left(H-h\right)\frac{k_{\mathrm{w}}}{\mu_{\mathrm{w}}}Q_{\mathrm{well}}}{h\frac{k_{\mathrm{nr}}}{\mu_{\mathrm{n}}}+\left(H-h\right)\frac{k_{\mathrm{w}}}{\mu_{\mathrm{w}}}}\right\}. \tag{35}$$

Define the following dimensionless variables, $\omega = \frac{h}{H}$, $\eta = \frac{r}{H}$ and, $\tau = \frac{Q_{\text{well}} t}{2\pi\phi(1-S_{wr})H^3}$. Using these in (35) gives

$$\frac{\partial\omega}{\partial\tau} = \frac{1}{\eta}\frac{\partial}{\partial\eta}\left\{\frac{\Gamma\lambda\omega\,(1-\omega)\,\eta\frac{\partial\omega}{\partial\eta} + (1-\omega)}{(\lambda-1)\,\omega+1}\right\}, \tag{36}$$

where

$$\lambda = \frac{\mu_{\text{w}}}{k_{\text{w}}}\frac{k_{\text{n}r}}{\mu_{\text{n}}}$$
$$\Gamma = \frac{2\pi\,\Delta\rho g H^2 k_{\text{w}}}{Q_{\text{well}}\mu_{\text{w}}}. \tag{37}$$

The mobility ratio for CO_2 and brine is λ and Γ is a dimensionless gravity number that represents the relative strength of buoyancy and viscous forces. Introducing the Boltzmann similarity transformation $\chi = \frac{\eta^2}{2\tau}$ into (36) leads to the following ordinary differential equation:

$$-\chi\frac{\mathrm{d}\omega}{\mathrm{d}\chi} = \frac{\mathrm{d}}{\mathrm{d}\chi}\left[\frac{2\Gamma\lambda\omega\,(1-\omega)\,\chi}{(\lambda-1)\,\omega+1}\frac{\mathrm{d}\omega}{\mathrm{d}\chi} + \frac{1-\omega}{(\lambda-1)\,\omega+1}\right]. \tag{38}$$

As shown in Fig. 1, the interface spans the entire aquifer thickness because CO_2 is injected uniformly across the aquifer. As a result, the boundary conditions are specified at $\omega = 0$ and $\omega = 1$. However, these values of ω occur at unknown values of the similarity variable, χ. Therefore, the boundary values of χ must be determined as part of the solution, as discussed in the following sections.

The similarity transformation requires a constant flow rate from the well so that Γ does not depend on time. The transformation also requires that the initial conditions are uniform, i.e., $\omega\,(\eta, 0) = 0$. Equation (38) describes a CO_2-brine displacement in terms of the dimensionless CO_2 depth of flow, ω, as a function of the similarity variable, χ, and two parameters, the mobility ratio and gravity number. The approximations and idealizations used to develop (38) have provided a significant simplification of the general two-phase flow problem that involves four unknowns (CO_2, brine pressures, and saturations) as functions of three spatial variables and time.

An important constraint is the balance between the total CO_2 injected and the volume of CO_2 present in the reservoir at any given time, which is given by

$$Q_{\text{well}} t = \phi\,(1-S_{wr})\,\pi\int_0^H r^2\,(h,t)\,\mathrm{d}h. \tag{39}$$

Note that for a given point in time, h only depends on r; therefore, this relationship can be inverted to express r as a function of h at any point in time.

Given the constant-density approximation for CO_2, this is equivalent to a total mass constraint on CO_2 in the reservoir. Recasting (39) in terms of the dimensionless variables gives the following total CO_2 mass condition:

$$\int_0^1 \chi\,\mathrm{d}\omega = 1. \tag{40}$$

4 Matched Boundary Extrapolation Solutions

There is no known general analytical solution to Eq. 38. In this section two approximate analytical solutions are developed using matched boundary extrapolations. As shown by Nordbotten and Celia (2006), as $\Gamma \to 0$,

$$\chi = \frac{\lambda}{\{1 + (\lambda - 1)\,\omega\}^2}, \tag{41}$$

For $0 \le \omega \le 1$. The condition $\Gamma \to 0$ leads to a first-order nonlinear wave equation for ω in terms of τ and η^2, which can be seen from Eq. 36. For $\Gamma > 1$, however, nonlinear diffusion effects become important and solutions are more difficult to determine.

To investigate solutions for other ranges of Γ and λ, integrate (38) from χ to χ_m, where $\chi_m = \chi\,(0)$:

$$\frac{\mathrm{d}\ln(\chi)}{\mathrm{d}\omega} = \frac{2\Gamma\lambda\omega\,(\omega - 1)}{\{(\lambda - 1)\,\omega + 1\}\int_0^\omega \chi\,\mathrm{d}\omega - \lambda\omega}. \tag{42}$$

The general approach is to use two asymptotic approximations for the integral term in (42) that are valid for $\omega \to 0$ and $\omega \to 1$, i.e., at the system boundaries. These approximations will be referred to as boundary solutions for the upper domain ($\omega \to 0$) and lower domain ($\omega \to 1$). The approximations need to be simple enough such that (42) can be solved analytically. These two boundary solutions are then extrapolated to a point in the interior where they are matched.

First consider the form of the integral in (42) that is consistent with the result in (41). This may be constructed by inserting (41) for χ in (42), except in the integral term. The result is

$$\int_0^\omega \chi\,\mathrm{d}\omega = \frac{\lambda\omega}{(\lambda - 1)\,\omega + 1}\left[\frac{\Gamma}{(\lambda - 1)}\{(\lambda - 1)\,\omega + 1\}(1 - \omega) + 1\right]. \tag{43}$$

Equation 43 reduces to 41 if the first term in the square bracket is small compared with 1, i.e., if $\frac{\Gamma}{\lambda - 1} \ll 1$ as $\omega \to 0$. Therefore, (41) provides a good approximation for the upper domain solution under these conditions as $\omega \to 0$ even if Γ is not small. The solution for conditions where $\frac{\Gamma}{\lambda - 1} \ll 1$ and $\lambda \gg 1$ are identified as MBE 1. For the purposes of the matched boundary extrapolations, (41) is generalized to the following form:

$$\chi = \frac{\chi_m}{\{1 + (\lambda - 1)\,\omega\}^2}. \tag{44}$$

This allows for flexibility in the solution relative to the total mass condition.

When $\frac{\Gamma}{\lambda - 1}$ is not small relative to 1, (44) is not applicable; nor is it applicable for $\lambda \le 1$. To extend the range of analytical approximations, consider a first-order approximation to the integral in (42) for small ω, i.e.,

$$\int_0^\omega \chi\,\mathrm{d}\omega \approx \chi_m\omega, \tag{45}$$

where χ_m is the unknown maximum value of χ at the top boundary, $\omega = 0$. Higher-order approximations to the integral in (45) were investigated but the net benefit did not seem to warrant the increased complexity in the analytical solution. Solutions using this approximation for the integral, for conditions when $\frac{\Gamma}{\lambda - 1} \gg 1$ and/or λ is small, are identified as MBE

2. More precise limits defining the applicable domains for MBE 1 and MBE 2 are discussed later.

Substituting (45) for the integral in (42) gives

$$\frac{\mathrm{d}\ln(\chi)}{\mathrm{d}\omega} = \frac{2\Gamma\lambda\omega(\omega-1)}{\{\lambda\omega+(1-\omega)\}\chi_m\omega-\lambda\omega}. \tag{46}$$

Solving (46) to first order as $\omega \to 0$ gives

$$\chi = \chi_m \exp\left(-\frac{2\Gamma\lambda\omega}{\chi_m-\lambda}\right). \tag{47}$$

Equations 44 and 47 represent boundary solutions for the upper domain for different ranges of the parameters Γ and λ. Equation 44 is based on a higher-order approximation to the integral in (42) as compared with (47), but is only valid for small ω if $\frac{\Gamma}{\lambda-1} \ll 1$ and $\lambda \gg 1$. Equation 47 will be used as the upper domain boundary solution for the other parameter ranges of Γ and λ.

For the lower domain, where $\omega \to 1$, the integral in (42) is approximated as 1. Thus, the total mass of the CO_2 is approximated as lying entirely within the upper domain with respect to the integral approximation. This means that the variation in the integral in the lower domain is small and its effects on the profile can be neglected; it does not mean that the resultant solution for χ is zero in the lower domain. With this approximation, Eq. 42 leads to the following result:

$$\chi = \chi_0 \exp\left(-\Gamma\lambda\omega^2\right), \tag{48}$$

Where χ_0, is an undetermined constant.

4.1 MBE 1 Solution

To produce a global solution, the upper and lower domain boundary solutions are matched at an interior point, ω_p in terms of the value of χ and the slope of the function, $\frac{\mathrm{d}\chi}{\mathrm{d}\omega}$. The MBE 1 solution is obtained using (44) and (48). To match these solutions at an interior point, equate the derivative of $\ln(\chi)$ for each of (44) and (48) and solve for ω_p:

$$\omega_p = \frac{1}{2(\lambda-1)}\left\{\sqrt{1+4\frac{(\lambda-1)^2}{\Gamma\lambda}}-1\right\}. \tag{49}$$

The solution is also required to be continuous at the match point. This is ensured by equating values of χ in (44) and (48) at $\omega = \omega_p$ and solving for χ_0:

$$\chi_0 = \frac{\chi_m \exp\left(\Gamma\lambda\omega_p^2\right)}{\left\{1+(\lambda-1)\omega_p\right\}^2}. \tag{50}$$

The total mass condition in (40) is used to determine χ_m by integrating (44) from $\omega = 0$ to $\omega = \omega_p$ and by integrating (48) using (50) from $\omega = \omega_p$ to $\omega = 1$:

$$\int_0^{\omega_p} \frac{\chi_m}{\{1+(\lambda-1)\omega\}^2}\mathrm{d}\omega + \int_{\omega_p}^{1} \frac{\chi_m \exp\left(\Gamma\lambda\omega_p^2\right)\exp\left(-\Gamma\lambda\omega^2\right)}{\left\{1+(\lambda-1)\omega_p\right\}^2}\mathrm{d}\omega = 1. \tag{51}$$

This results in the following for χ_m:

$$\chi_m = \left[\left\{ \frac{\omega_p}{1+(\lambda-1)\,\omega_p} \right\} + \frac{\sqrt{\pi}}{2\sqrt{\Gamma\lambda}} \frac{\exp\left(\Gamma\lambda\omega_p^2\right)}{\left\{1+(\lambda-1)\,\omega_p\right\}^2} \left\{ \operatorname{erf}\left(\sqrt{\Gamma\lambda}\right) - \operatorname{erf}\left(\sqrt{\Gamma\lambda}\omega_p\right) \right\} \right]^{-1}. \tag{52}$$

If $\omega_p > 1$, then the upper domain solution applies over the entire domain and

$$\chi_m = \lambda. \tag{53}$$

If $\omega_p < 0$, then the lower domain solution applies over the entire domain and

$$\chi_m = \frac{2\sqrt{\Gamma\lambda}\lambda^2}{\sqrt{\pi}\operatorname{erf}\left(\sqrt{\Gamma\lambda}\right)}. \tag{54}$$

The first matched boundary extrapolation solution, or MBE 1, is given by Eq. 44 for the upper domain and (48) for the lower domain. The value of χ_0 in (48) is given by (50) and the value of χ_m in both (44) and (50) is given by (52), (53), or (54), depending on the value of ω_p. The upper domain applies to values of ω from 0 to the match point, ω_p, and for the lower domain, from ω_p to 1, where ω_p is given by (49).

4.2 MBE 2 Solution

The same procedure is applied to match the upper domain solution (47) with the lower domain solution (48). Equating the derivative of $\ln(\chi)$ for each at the match point, ω_p gives

$$\omega_p = \frac{1}{\chi_m - \lambda}. \tag{55}$$

To ensure continuity of the upper and lower domain solutions at the match point, equate values of χ in (47) and (48) at the match point and solve for χ_0:

$$\chi_0 = \chi_m \exp\left\{ -\frac{\Gamma\lambda}{(\chi_m-\lambda)^2} \right\}. \tag{56}$$

Finally, the total mass constraint is used to determine χ_m. Integrating (47) from $\omega = 0$ to $\omega = \omega_p$ and by integrating (48) using (56) from $\omega = \omega_p$ to $\omega = 1$ gives

$$\chi_m \int_0^{\frac{1}{\chi_m-\lambda}} \exp\left(\frac{-2\Gamma\lambda\omega}{\chi_m-\lambda}\right) \mathrm{d}\omega + \chi_m \exp\left\{ -\frac{\Gamma\lambda}{(\chi_m-\lambda)^2} \right\} \int_{\frac{1}{\chi_m-\lambda}}^{1} \exp\left(-\Gamma\lambda\omega^2\right) \mathrm{d}\omega = 1. \tag{57}$$

Simplifying Eq. 57 gives

$$\chi_m \left(\frac{\chi_m-\lambda}{2\Gamma\lambda}\right) \left\{ 1 - \exp\left(\frac{-2\Gamma\lambda}{(\chi_m-\lambda)^2}\right) \right\} + \chi_m \left(\frac{\sqrt{\pi}}{2\sqrt{\Gamma\lambda}}\right) \exp\left\{ -\frac{\Gamma\lambda}{(\chi_m-\lambda)^2} \right\} \left\{ \operatorname{erf}\left(\sqrt{\Gamma\lambda}\right) - \operatorname{erf}\left(\frac{\sqrt{\Gamma\lambda}}{\chi_m-\lambda}\right) \right\} = 1. \tag{58}$$

Table 1 Summary of solution domains

	$\lambda \leq 2$	$\lambda > 2$
$\Gamma/(\lambda - 1) \leq 1/15$	MBE 2	MBE 1
$1/5 \leq \Gamma/(\lambda - 1)$	MBE 2	MBE 2
$1/15 < \Gamma/(\lambda - 1) < 1/5$	MBE 2	Transition (weighted average of MBE 1 and MBE 2)

Although Eq. 58 must be evaluated numerically to determine χ_m, finding the root of this transcendental equation is a much simpler numerical problem than solving the second-order nonlinear differential equation given by Eq. 38. In some cases, ω_p can be greater than 1, meaning that the upper domain solution is used for the entire domain. For these cases, (58) becomes

$$\chi_m \left(\frac{\chi_m - \lambda}{2\Gamma\lambda} \right) \left\{ 1 - \exp\left(\frac{-2\Gamma\lambda}{(\chi_m - \lambda)} \right) \right\} = 1. \tag{59}$$

The second matched boundary extrapolation solution, or MBE 2, is given by Eq. 47 for the upper domain and (48) for the lower domain. The value of χ_0 in (48) is given by (56) and the value of χ_m in both (47) and (56) is given by (58) or (59), depending on the value of ω_p. The upper domain is used for values of ω from 0 to the match point, ω_p, and for the lower domain, from ω_p to 1, where ω_p is given by (55).

4.3 MBE 1 and MBE 2 Solution Domains and Transition

MBE 2 is found to be applicable for all cases with $\lambda \leq 2$. For $\lambda > 2$, comparisons of the MBE solutions with numerical solutions of Eq. 41 show that the applicability of MBE 1 and MBE 2 transitions near $\frac{\Gamma}{\lambda-1} = \frac{1}{10}$. For $\frac{\Gamma}{\lambda-1} \leq \frac{1}{15}$ and $\lambda > 2$, MBE 1 is applicable. For $\frac{1}{5} \leq \frac{\Gamma}{\lambda-1}$ and $\lambda > 2$, MBE 2 is applicable. For the transition zone $\frac{1}{15} < \frac{\Gamma}{\lambda-1} < \frac{1}{5}$, a weighted average solution, $\overline{\chi}$, is used to provide a smooth transition:

$$\overline{\chi} = \frac{\lambda - 1 - 5\Gamma}{10\Gamma}\chi_1 + \frac{15\Gamma - \lambda + 1}{10\Gamma}\chi_2, \tag{60}$$

where χ_1 is the MBE 1 solution and χ_2 is the MBE 2 solution. A transition between $\lambda \leq 2$ and $\lambda > 2$ is not needed because the transition is smooth except for conditions in which $\frac{\Gamma}{\lambda-1} \leq \frac{1}{15}$. At the transition point, $\lambda = 2$, occurs for small values of Γ, $\Gamma \leq \frac{1}{15}$. For this range of the parameters, differences between the MBE 1 and MBE 2 solutions are not large. A summary of the solution domains is given in Table 1.

5 Comparison of Results

The results of the match boundary expansions are compared in this section with the numerical solution of Eq. 42 as well as other approximate solutions documented by Nordbotten and Celia (2006) and Dentz and Tartakovsky (2009a). The comparison is performed over a range of mobility ratios, λ, from 0.1 to 100 and gravity numbers, Γ, also from 0.1 to 100. The range of mobility ratios covers conditions in which the injected fluid is less mobile than the resident fluid in the reservoir ($\lambda < 1$) to cases where the injected fluid is more mobile than the resident fluid ($\lambda > 1$). Typically, CO_2 injected into a brine reservoir falls in the latter category for mobility ratios. The range of gravity numbers covers conditions where viscous

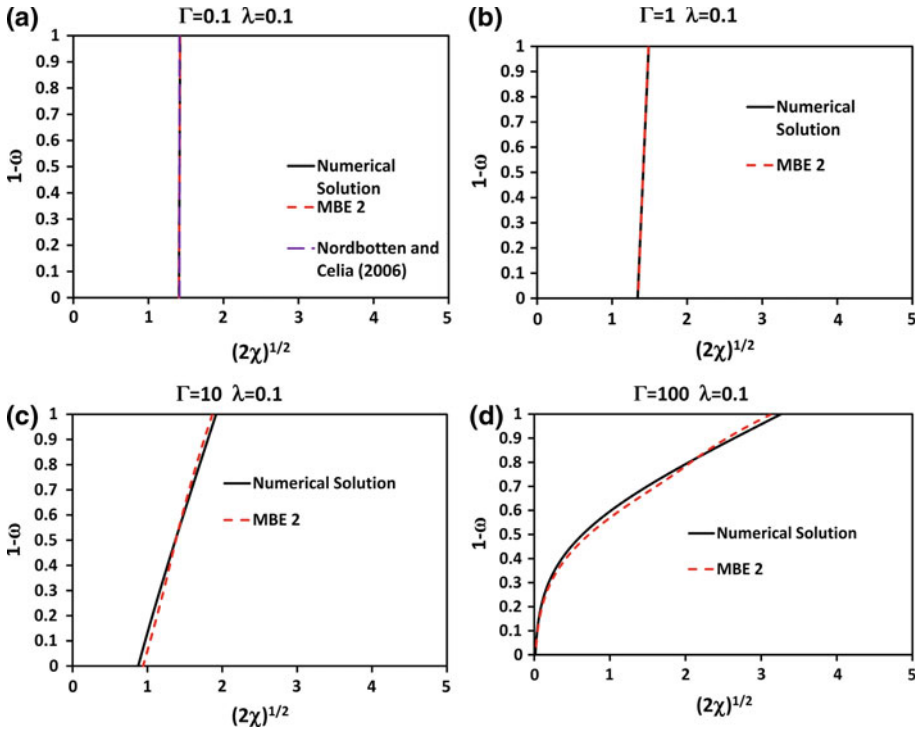

Fig. 2 Comparison of solutions for $\lambda = 0.1$; Γ: **a** 0.1, **b** 1, **c** 10, **d** 100

forces are dominant relative to buoyancy forces $\Gamma < 1$ to cases where buoyancy forces are dominant $\Gamma > 1$. Because Γ depends on the injection rate, aquifer permeability and aquifer thickness, it is possible for CO_2 injection to fall under different flow regimes with respect to Γ. The suite of MBE solutions are used over the entire parameter space, but Nordbotten and Celia (2006) and Dentz and Tartakovsky (2009a) solutions only apply over a portion of the parameter space.

The numerical solution is obtained using Eq. 42. An initial value of χ_m is estimated and then the solution may be computed using explicit stepping in ω. Then, the mass balance condition, Eq. 40, is checked and χ_m is adjusted with the goal of bringing the mass balance condition closer to 1 in the next iteration. The solution can become unstable if χ_m is too small, generating an erratic profile of χ as a function of ω. In these cases, stability is restored by taking the next estimate of χ_m closer to a previous value of χ_m that generated a stable profile.

The Nordbotten and Celia (2006) solution for $\Gamma < 1$ is given by Eq. 41. The Dentz and Tartakovsky (2009a) solution applies for buoyancy-dominated cases (Dentz and Tartakovsky 2009b), which implies $\Gamma > 1$. The use of this solution is further restricted to cases with $\lambda > 1$ as investigated by Dentz and Tartakovsky (2009a). Expressed in the notation of this article, the Dentz and Tartakovsky (2009a) solution is

$$\chi = \left(\frac{2\Gamma\lambda}{\lambda - 1}\right)\left\{\exp\left(\frac{2\Gamma\lambda}{\lambda - 1}\right) - 1\right\}^{-1} \exp\left\{\frac{2\Gamma\lambda\,(1-\omega)}{\lambda - 1}\right\}. \tag{61}$$

Cases with $\lambda = 0.1$ are shown in Fig. 2. The mobility of CO_2 is always less than that of brine, such that $\lambda = 0.1$ is not expected for CO_2-brine displacements. However, such conditions

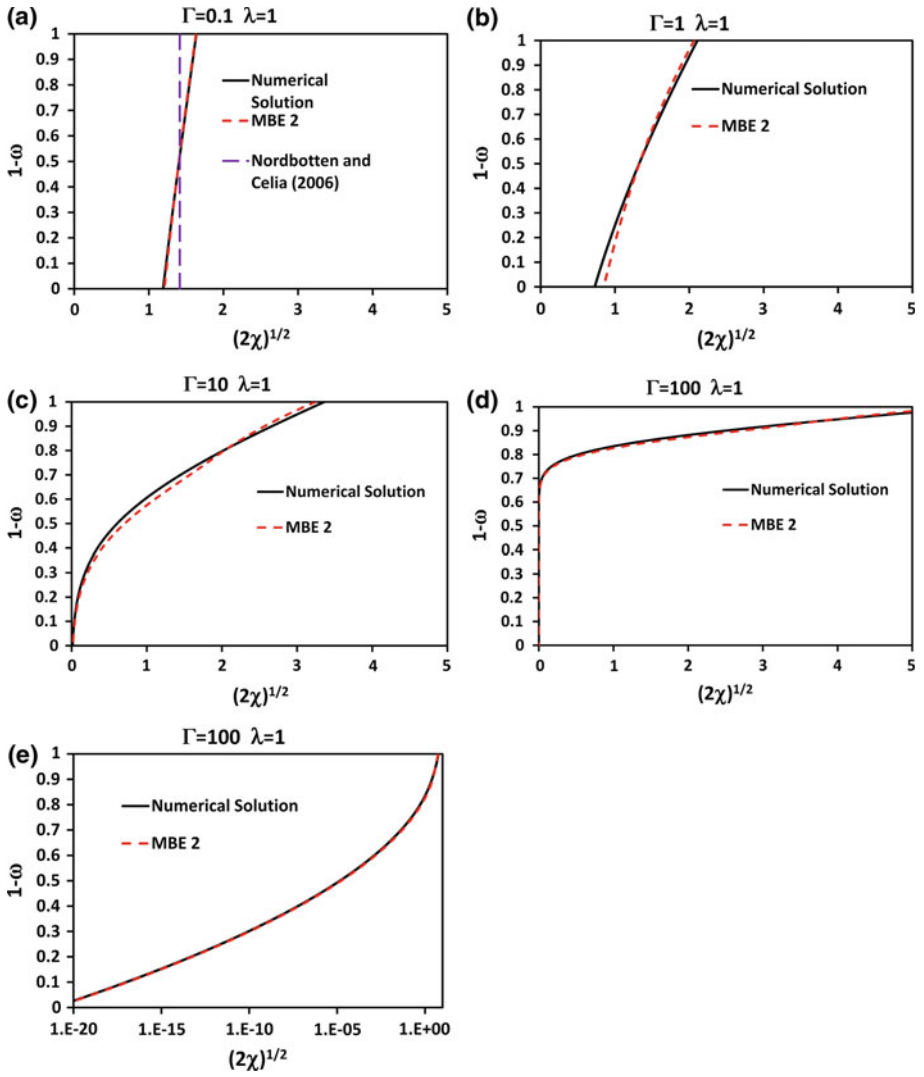

Fig. 3 Comparison of solutions for $\lambda = 1$; Γ: **a** 0.1, **b** 1, **c** 10, **d, e** 100

are expected for brine displacing CO_2, as would occur if a water-alternating-gas injection process were used (Juanes et al. 2006). The solutions are plotted using the dimensionless variable $(2\chi)^{1/2}$ which is proportional to the radial distance from the well and $1-\omega$, which is proportional to the vertical distance from the base of the reservoir. The Nordbotten and Celia (2006) solution, which applies for the case with $\Gamma = 0.1$, results in a piston-like displacement for $\lambda \leq 1$. MBE 2 is applicable for this value of λ.

Cases with $\lambda = 1$ are shown in Fig. 3. As for $\lambda = 0.1$, the Nordbotten and Celia (2006) solution, which applies for the case with $\Gamma = 0.1$, results in a piston-like displacement. MBE 2 is applicable for this value of λ. The case $\Gamma = 100$ is also shown in Fig. 3e on a logarithmic scale because of the poor resolution for $1 - \omega < 0.6$ in Fig. 3d.

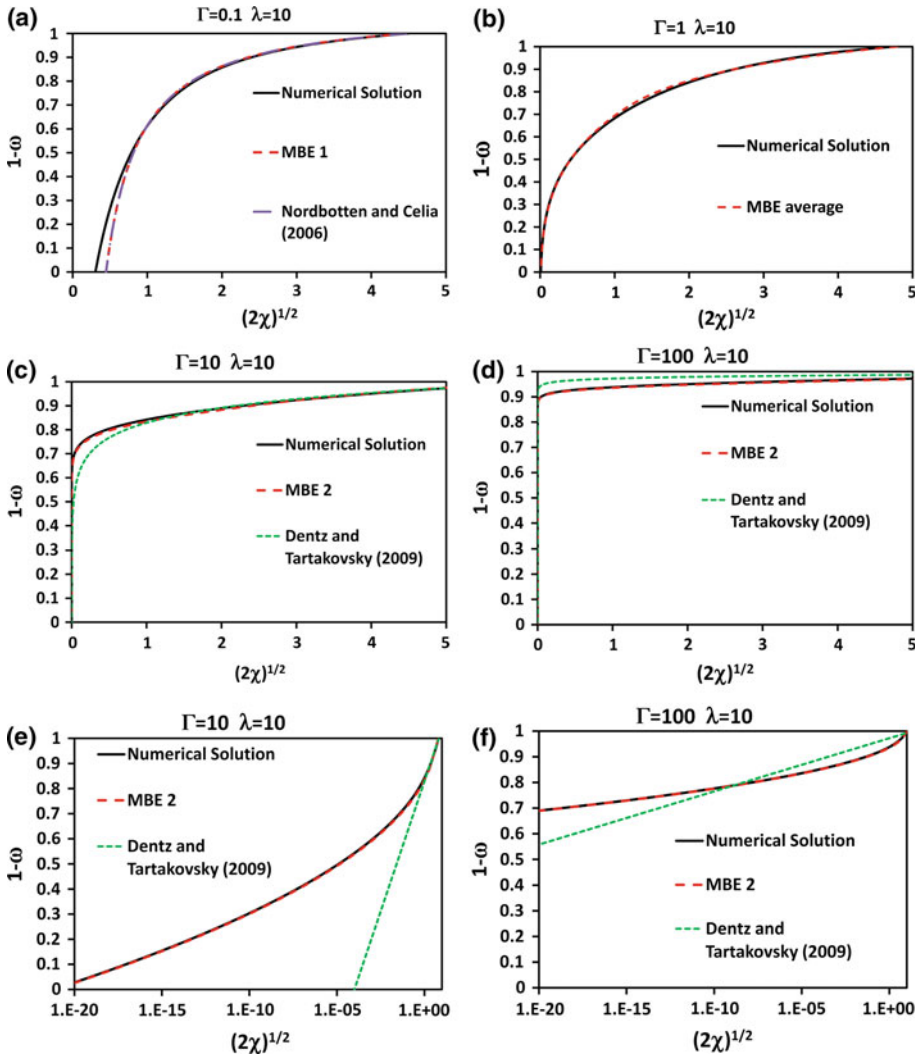

Fig. 4 Comparison of solutions for $\lambda = 10$; Γ: **a** 0.1, **b** 1, **c, e** 10, **d, f** 100

Cases with $\lambda = 10$ are shown in Fig. 4. The solution proposed by Nordbotten and Celia (2006) applies here for $\Gamma = 0.1$, and the solution proposed by Dentz and Tartakovsky (2009a) is applicable to cases with $\Gamma = 10$ and $\Gamma = 100$. As expected, the Nordbotten and Celia (2006) solution is found to be more accurate for smaller values of the gravity number; the Dentz and Tartakovsky (2009a) solution becomes more accurate for higher gravity number conditions, consistent with the findings reported by Vilarrasa et al. (2010). The MBE 1 solution applies for the $\Gamma = 0.1$ case and is found to be nearly identical to the Nordbotten and Celia (2006) solution. The $\Gamma = 1$ case falls into the transition zone between MBE 1 and MBE 2 solutions where the weighted average solution is used. MBE 2 solutions apply for $\Gamma = 10$ and 100, which are also shown against a logarithmic scale in Fig. 4e, f.

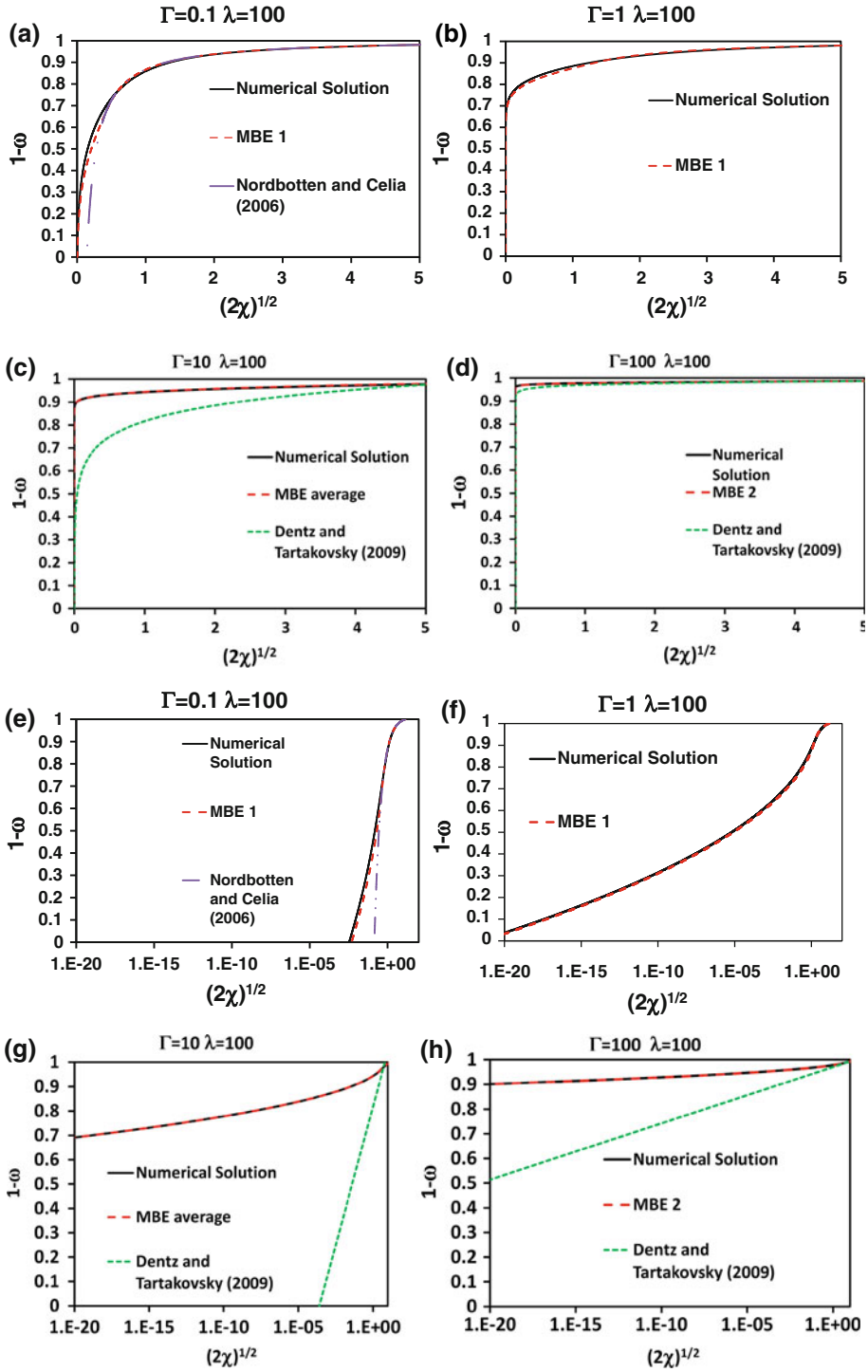

Fig. 5 Comparison of solutions for $\lambda = 100$; Γ: **a, e** 0.1, **b, f** 1, **c, g** 10, **d, h** 100

Cases with $\lambda = 100$ are shown in Fig. 5. As for $\lambda = 10$, the solution proposed by Nordbotten and Celia (2006) applies here for $\Gamma = 0.1$ and the solution proposed by Dentz and Tartakovsky (2009a) is applicable for cases with $\Gamma = 10$ and $\Gamma = 100$. The MBE 1 and Nordbotten and Celia (2006) solutions are nearly identical for $\Gamma = 0.1$ when $1 - \omega > 0.5$. For the case with $\Gamma = 1$, the MBE 1 solution applies because $\lambda - 1$ is larger than 15Γ. The MBE average solution applies for $\Gamma = 10$, while the MBE 2 solution applies for $\Gamma = 100$. Logarithmic plots are provided for all of these cases in Fig. 5e through h, respectively. It should be noted that cases with small values of Γ and large values of λ lead to greater sensitivity to the value of χ at $\omega = 0$, which impacts the development of the numerical solution. For the extreme case $\Gamma = 0.1$ and $\lambda = 100$ the solution required a value of χ_m that was correct to more than 30 significant digits to obtain the converged numerical solution profile shown in Fig. 5a, e.

In general, the MBE suite of solutions is found to be in close quantitative agreement with the numerical solution over the entire parameter space.

6 Summary and Conclusions

A dimensional analysis of the governing equations has shown that for radial injection or release of CO_2 from a well into a saline reservoir, a CO_2—brine displacement process will always tend to a vertical equilibrium/gravity segregation condition after a sufficiently long time. Vertical equilibrium tends to occur when the displacement distance is large relative to the aquifer thickness but is inhibited by a low vertical-to-horizontal permeability ratio. However, because the displacement distance increases with time, vertical equilibrium will tend to be a better approximation with increasing time. Gravity segregation will occur when buoyancy dominates viscous forces and capillary forces. As for vertical equilibrium, this approximation becomes better with increasing time, provided that capillary forces are small relative to buoyancy forces. Capillary forces may be neglected relative to buoyancy forces for sufficiently large values of the dimensionless Bond number. The strength of capillary forces relative to buoyancy forces does not, however, diminish with increasing time.

Approximate analytical/semi-analytical solutions were developed for radial displacement of brine by CO_2 entering a homogeneous, horizontal aquifer from a fully penetrating well. The process was approximated using vertical equilibrium, complete gravity segregation, and incompressibility. Solutions that represent CO_2—brine interface behavior near the upper and lower reservoir boundaries were extrapolated to an interior point where the solutions were matched and constrained using overall CO_2 mass balance to produce global approximations. Two solutions were derived based on different boundary solutions for the upper domain, which apply for different ranges of the gravity number and mobility ratio. The combined set of solutions significantly extends the range and improves the accuracy of existing analytical approximations for describing radial CO_2—brine displacement processes.

Acknowledgements The initial draft of this article was carefully reviewed by Drs. Abdullah Cihan and Dan Hawkes. This study was supported by the Assistant Secretary for Fossil Energy, Office of Sequestration, Hydrogen, and Clean Coal Fuels, National Risk Assessment Partnership, Project No. AA1505000, of the U.S. Department of Energy under Contract No. DE-AC02-05CH11231.

References

Bear, J.: Dynamics of Fluids in Porous Media. American Elsevier Publishing Company Inc., New York (1972)

Dentz, M., Tartakovsky, D.: Abrupt-interface solution for carbon dioxide injection into porous media. Transp. Porous Med. **79**, 15–27 (2009a)

Dentz, M., Tartakovsky, D.: Response to "Comments on Abrupt-Interface Solutionfor Carbon Dioxide Injection into Porous Media by Dentz and Tartakovsky (2008)" by Lu et al. Transp. Porous Med. **79**, 39–41 (2009b)

IPCC: IPCC special report on Carbon dioxide capture and storage. Prepared by working group III of the intergovernmental panel on climate change [Metz, B.O., Davidson, H.C., de Coninck, M.L., Meyer, L.A. (eds.)]. Cambridge University Press, Cambridge/New York (2005)

Juanes, R., Spiteri, E.J., Orr, F.M. Jr., Blunt, M.J.: Impact of relative permeability hysteresis on geological CO_2 storage. Water Resour. Res. **42**, W12418 (2006)

Liu, Y., Wang, L., Yu, B.: Sharp front capturing method for Carbon dioxide plume propagation during injection into a deep confined aquifer. Energy Fuels **24**, 1431–1440 (2010)

Nordbotten, J.M., Dahle, H.K.: Impact of capillary forces on large-scale migration of CO_2. XVIII International Conference on Water Resources, CMWR, Barcelona (2010)

Nordbotten, J.M., Celia, M.A.: Similarity solutions for fluid injection into confined aquifers. J. Fluid Mech. **561**, 307–327 (2006)

Nordbotten, J.M., Celia, M.A., Bachu, S.: Injection and storage of CO_2 in deep saline aquifers: analytical solution for CO_2 plume evolution during injection. Trans. Porous Med. **58**(3), 339–360 (2005)

Vilarrasa, V., Bolster, D., Dentz, M., Olivella, S., Carrera, J.: Effects of CO_2 compressibility on CO_2 storage in deep saline aquifers. Transp. Porous Med. (2010). doi:10.1007/s11242-010-9582-z

Yortsos, Y.C.: A theoretical analysis of vertical flow equilibrium. Trans. Porous Med. **18**, 107–129 (1995)